JOURNAL OF MARITIME RESEARCH

Vol XX. No. I (2023) pp 59–74

ISSN: 1697-4840, www.jmr.unican.es

Numerical prediction of the ship-to-ship interaction during lighter-ing operations

R. Ali[1,*]

ARTICLE INFO

Article history:
Received 19 Jan 2023;
in revised from 22 Jan 2023;
accepted 03 Feb 2023.

Keywords:
Lightering operation, Hydrodynamic interaction, RANS, CFD, OPENFOAM.

ABSTRACT

A series of systematic simulations were carried out to study the effect of the relative longitudinal and lateral spacing on the ship-to-ship hydrodynamic interaction during lightering operations. The simulations were performed on two KVLCC2 hulls advancing parallel in deep still water at a low Froude number. The simulation was carried out using OPENFOAM, turbulence was modeled using RANS, the k- SST turbulent model was used to close RANS equations. The validity of the numerical configurations was examined by a published experimental benchmark, the numerical-experimental comparison revealed a good agreement. The surface pressure distribution and the wave pattern surrounding both hulls were presented and analyzed for various relative positions. The changes in the hydrodynamic interaction forces and moments, as a function of the longitudinal and lateral spacings, were computed and analyzed. The positive relative longitudinal position extending to 15% was found to be suitable for conduction lightering operation.

1. Introduction.

Although the ship spends most of her life sailing in open waters, the cases in which she is subjected to the presence of a close rigid boundary are not few, such as sailing in restricted areas, overtaking or encountering other marine objects at small lateral distances, and other investment operations such as lightering operations and ship-tug maneuvering.

Sailing close to a rigid boundary changes the pressure and velocity fields surrounding the hull, leading to a distinct change in the forces and moments acting on it, which can cause perilous situations. So, studying this special case and evaluating the mutual hydrodynamic effect is extremely important. Various approaches were used to study the ship hydrodynamic interaction with rigid boundaries. Using the potential method, (Xiang and Faltinsen, 2010) investigated the maneuvering of two interacting ships travelling at low Froude numbers $Fr < 0.2$ in calm water of infinite horizontal extent. Maneuvering hydrodynamic forces and moments were obtained by a developed method based on assumptions of 3D potential flow. The method was verified and validated by (de Decker B, 2006) experimental results as well as (WANG, 2007) potential results which found to give a good agreement, but effects of sea waves, wind and current were not treated. (Yao and Zou, 2010) used the panel method to calculate the sinkage and trim of a ship sailing in a shallow channel. Numerical calculations were performed on Series 60 ship using a Green function of Rankine type. The vertical force and pitching moment were obtained by integrating the hydrodynamic pressure over the hull surface, the sinkage and trim were calculated according to dynamic equilibrium, in the end the numerical results were validated against the experimental data and found to be in a good agreement. (Yuan et al., 2015; Yuan and Incecik, 2016), carried out their research to predict the effect of forward speed on ship-to-ship interaction forces, moments, and wave elevations during overtaking maneuvering in shallow water. MHydro, a software based on the 3D Rankine source method was used. The accuracy of the numerical predicted results revealed a high sensitivity towards the panel size and ship forward speed. However, the results were

[1]Department of Hydroaeromechanics and Marine Acoustics, St. Petersburg State Marine Technical University (SMTU), Saint-Petersburg, 190121, Russia.
*Corresponding author: R. Ali. E-mail Address: ramimamdouhali@gmail.com.

compared with model tests as well as the published CFD results and showed a satisfied agreement. (Yu et al., 2019) studied the interactions between two ships during calm-water moderate-speed overtaking maneuvers in a deep water in two ways: computationally by a potential-flow panel method, and experimentally by towing-tank tests. They reported that when two ships travel at comparable speeds, the interference of ship waves considerably changes the free-surface elevations between the two vessels. Consequently, the hydrodynamic loads on both vessels are considerably affected by the uneven free-surface elevations around their hulls. (Skejic et al., 2011), based on the three-dimensional potential flow theory, carried out a theoretical investigation of underway lightering maneuver in calm and deep water. They reported that: when using the potential theory to study the hydrodynamic interaction effects between ships of modern hull forms, the three-dimensional method should be a preferable choice compared to the analytical methods based on the assumption of the near-field slender-body theories. (Serban, 2015) studied the ship-to-ship interaction between a bulk carrier and an oil tanker passing through a narrow waterway in Suez Canal. Their results showed that the yaw moment and lateral force are strong enough to veer the course of the smaller ship into the adjacent bank.

When it comes to viscous approaches, various situations were studied, such as interacting during overtaking maneuvers, interacting between passing and moored ships, and interacting between two ships traveling parallel. (Wnęk et al., 2018) studied the hydrodynamic interaction (surge, sway forces and yaw moment) between two ship models, which are widely different in their dimensions (a tug and a tanker), advancing in still water parallel to each other with different lateral distances and two different values of the fluid depth. For each depth, CFD Computations were carried out with four different flow models, viscous and inviscid flow with double hull and free surface case. the results showed a fair agreement with both available experimental data and panel method results. The study concluded that the viscosity has a comparatively weak influence, while at the same time the wave-making effects are important especially at small clearance between ships. (Benedict et al., 2011) used the overset mesh technique to study the interaction phenomena between two ships sailing in parallel during overtaking maneuvering. The results were compared with the experimental data and showed a good overall agreement, but an exception to this general agreement is the clear discrepancy between the results and experimental data at some specific relative positions of the interacting ships. (Zhang and Zou, 2011) investigate the encountering and overtaking maneuver in shallow water at low Froude numbers using FLUENT packet with dynamic mesh technique. The sway forces and yaw moment coefficients were calculated for different values of canal width, effects of canal depth and lateral distance to the bank were also studied. (Sian et al., 2016) investigated the overtaking maneuver in shallow water between an LNG and a Series 60 model. A computational domain of two million cells was simulated with Fluent CFD packet using the k−ω SST turbulence model. The experimental and numerical results showed rather satisfied agreement with moderate under- or over-prediction for some cases. (Nandhini and Nallayarasu, 2020) studied the interaction forces between a passing ship and a moored ship. Initially, the CFD simulation was validated against existing experimental data and then extended to include a number of parameters such as displacement, speed and lateral distance of the passing ship. It was found that the longitudinal and lateral forces acting on the moored ship become negligible when the lateral distance is more than three times the width of the ship.

Most of the reviewed studies investigated the hydrodynamic interaction between ships of vastly different size, or between ships moving at different speeds, which is not the case during lightering operation. Furthermore, the longitudinal space in some cases exceeded the cargo transfer limit between ships.

In this paper, the viscous fluid flow around two close ships advancing in calm and deep water in parallel course at the same constant low speed were simulated. Wide range of lateral and longitudinal distances were tested, their effects on the interaction forces and moments were obtained, surface pressure distribution and wave contour around the hulls were analyzed. The paper starts by defining the problem in section 2, which includes a brief description of the geometrical and operational characteristics of the kvlcc2 hull, governing equations, and turbulence modeling approaches. Then, a detailed review of the computational domain, mesh specifications, numerical settings, and boundary conditions are described in section 3. Validation with experimental data is subsequently performed. Finally, results and discussion of the effect of lateral and longitudinal distance on flow characters and interaction between ships are discussed in the sections 4 and conclusions are presented in section 5.

2. Problem definition.

2.1. Hull form.

Figure 1: Body plan and geometry of the KVLCC2.

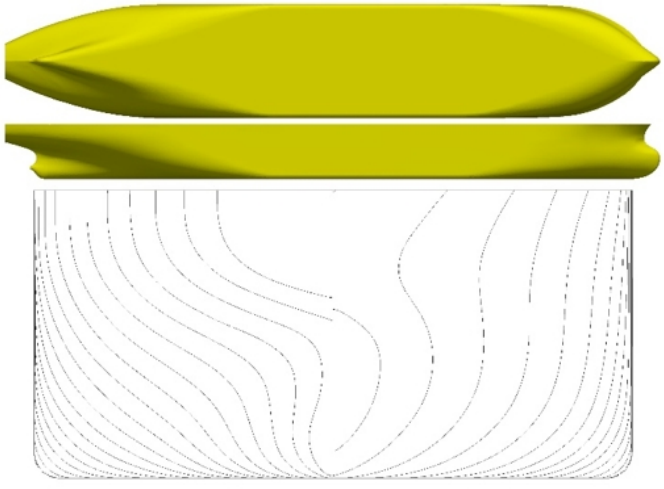

Source: Authors.

The ship under consideration is the second variant of the MOERI tanker, the Very Large Crude Carrier (KVLCC2), a

tanker ship with bulbous bow, U-shaped stern frame-lines and low service speed of 15.5 kt. Being a tanker makes it very suitable for lightering operation study. In addition to that, KVLCC2 is a well-known hull form with abundance in experimental results of resistance and is widely used as a benchmark case for the CFD validation.

During lightering operation, the ships are generally of the same type but of different lengths. Therefore, two different scaled model 1/75 and 1/106 of KVLCC2 will be used. It is worth noting that the type and dimensions were not chosen arbitrarily, but rather chosen in accordance with the models and dimensions used in the experimental work of (de Decker B, 2006).

The hull shape of the KVLCC2, and the principles dimensions and coefficients of the original, as well as the two scaled models, are shown in Fig. 1 and Table 1, respectively.

2.2. Axis Conventions.

Two sets of parallel right-handed coordinate systems are used, the earth-fixed coordinate system $O(X, Y, Z)$ and two moved coordinate systems $O_i(x, y, z)$.

The moved coordinate system $O_i(x, y, z)$ is linked to each ship with the x-axis pointing forward, y-axis to the port side, and the z-axis upwards. Its origin is defined as the intersection of the center-plane, midship plane, and water-plane.

The earth-fixed coordinate system is used to identify the coordinate of COG of each ship at start time, while the moved coordinate system will be used to define the relative position of each ship to another one, as well as to determine the direction of the interaction forces and moments acting on both ships.

In the comparative experimental work conducted by Decker, z-axis was oriented downward. So, during the validation stage, the directions of the obtained forces and moments will be corrected to conform to the decker convention.

The corresponding right-handed coordinate systems and the positive signs convention of the hydrodynamic interaction forces and moments are shown in Fig. 2.

Figure 2: Coordinate system and signs conventions.

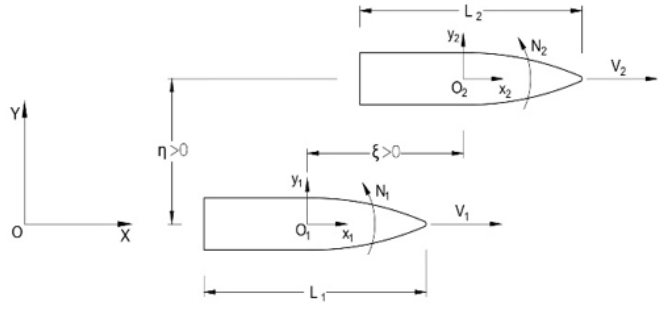

Source: Authors.

2.3. The non-dimensionality.

The service ship SS and the ship to be lightered STBL will travel in a parallel course at equal speed v without drift. The SS is always located on the port-side of the STBL, her position is defined by the origin location of her moving coordinate system in the STBL moving coordinate system.

To describe the case clearly and to reduce the number of variables associated with it, the relative position of the two ships is defined non-dimensionally as follows:

- The non-dimensional lateral distance (η),$\eta = \partial y / B_{avg}$where dy is the lateral distance between the centerlines of the ships, B_{avg} is the average molded breadth of the SS and STBL.
- The non-dimensional longitudinal distance (ξ),$\xi = \partial x / L_{avg}$ where dx is the longitudinal distance between the midsections of the ships, L_{avg} is the average length between perpendiculars of the SS and STBL.

Obviously, when the interacted ships float in symmetry position, their midship planes coincide and so the $\xi = 0$.

The hydrodynamic resistance forces F_x, lateral forces F_y and the yaw moment N acting on the COG of both ships will be presented non-dimensionally as follows:

$$C_x = F_x/(0.5 \cdot \rho \cdot B \cdot T \cdot v^2)$$

$$C_y = F_y/(0.5 \cdot \rho \cdot L_{pp} \cdot T \cdot v^2)$$

$$C_n = M_z/(0.5 \cdot \rho \cdot L_{pp} \cdot B \cdot T \cdot v^2)$$

Where, L_{PP}, B, T are the main dimension of STBL model, v $[m/sec]$ is flow velocity in model scale.

In this study, both models proceed at the same constant full-scale speed $v = 4$ $[Knot]$, the corresponding constant speed on STBL model scale is 0.237 $[m/sec]$, Froude number for the STBL and SS are 0.037 and 0.044 respectively. The lateral distance η and the longitudinal distance ξ are varied systematically so the SS covered all the possible location near the STBL. The numerical values for all parameters are given in Table 2.

2.4. Governing Equations, Turbulence Model.

The continuity equation and the Navier-Stokes equations are the basic equations governing fluid flow. The differential forms of these equations are:

$$\frac{\partial \rho}{\partial t} + \frac{\partial (\rho u_i)}{\partial x_i} = 0$$

$$\frac{\partial (\rho u_i)}{\partial t} + \frac{\partial (\rho u_j u_i)}{\partial x_j} = \rho g_i - \frac{\partial p}{\partial x_i} + \mu \frac{\partial^2 u_i}{\partial x_j{}^2}$$

Where ρ is the density, μ is the dynamic viscosity, p is the pressure, u_i is the velocity vector and $x_{i,j}$ is the spatial vector.

Together, they form a set of coupled, non-linear partial differential equations (PDEs), which can be solved analytically for only a very limited number of simple cases. For complex cases, numerical methods are used to discrete the differential equations over the studied domain, and then the resultant system of linear algebraic equations are solved using a suitable matrix solution method. The Finite Volume Method (FVM) is among the most widely used numerical methods in fluid dynamics.

Table 1: Main particulars of the ship models.

	Full-scale	CFD		Experiments	
Scale	1.000	1/75	1/106	1/75	1/106
Main particulars	**Original Full-scale**	**STBL**	**SS**	**STBL**	**SS**
Lpp (m)	320.0	4.2360	3.0190	4.2360	3.0190
Lwl (m)	325.5	4.3088	3.0709	-	-
Bwl (m)	58.0	0.7678	0.5472	0.7640	0.5140
D (m)	30.0	0.3971	0.2830	-	-
T full (m)	20.8	0.2753	0.1962	0.2670	0.1980
Displacement (m^3)	312622	0.7252	0.2625	0.6850	0.2550
S w/o rudder (m^2)	27194	4.7652	2.4205	-	-
CB	0.8098	0.8098	0.8098	0.792	0.830
CM	0.9980	0.9980	0.9980	-	-
LCB (%), fwd+	3.48	3.48	3.48	-	-
LCG (m)	11.1	0.1474	0.1051	-	-
GM (m)	5.71	0.076	0.054	-	-
ixx/B	0.40	0.40	0.40	-	-
iyy/Lpp	0.25	0.25	0.25	-	-
izz/Lpp	0.25	0.25	0.25	-	-

Source: Authors.

Table 2: Set of lateral and longitudinal distances.

F_r	η				ξ						
0.037	1.06	1.2	1.4	1.8	-0.5	-0.3	-0.15	0	0.15	0.3	0.5

Source: Authors.

As it is known, turbulent flow around the ships is highly unsteady, irregular and characterized by a wide range of different length and velocity scales. Capturing all the turbulent scales requires a very fine mesh and so a huge number of computational cells, which consumes a lot of time and resources. To overcome this problem, many methods were introduced to describe the turbulent flow based on simplified assumptions as Large Eddy Simulation (LES), Detached Eddy Simulation (DES) and Reynolds-averaged Navier-Stokes (RANS).

RANS is the most used approach in engineering practice nowadays. However, it is the fastest and the least consuming of computational resources. According to RANS the averaged continuity and the momentum equations for incompressible flow are written as follows:

$$\frac{\partial \overline{u}_j}{\partial x_j} = 0$$

$$\rho \frac{D\overline{u}_i}{Dt} = F_i - \frac{\partial \overline{p}}{\partial x_i} + \frac{\partial}{\partial x_j}\left(\tau_{ij} - \rho\overline{u'_i u'_j}\right)$$

Where: τ_{ij} is the viscous stress, while $\rho\overline{u'_i u'_j}$ is the Reynolds stress.

The Reynolds stress term in RANS equations breaks the system closure. Turbulence modeling is only an attempt to close the RANS equation and to predict Reynolds stress values. In this paper, the KW-SST turbulent model with a wall function near-wall treatment approach will be used.

3. Numerical formulation.

3.1. Computational Domain.

A box-shaped domain was chosen to conduct the entire series of simulations. The computational domain's dimensions were chosen according to ITTC recommendations. The computational domain consists of eight boundaries: the inlet plane, outlet plane, atmosphere plane, bottom, two side planes and two hull surfaces. The inlet plane is located at 2L in front of STBL, while the outlet plane is located at 5L behind it, and the domain width is extended laterally by 2L away from the model hull. The air and water phases are extended to a distance of 2L from the still water-free surface.

Figure 3: Overview of the computational domain and Grid structure around STBL and SS. (a) Computational domain. (b) Free surface and near hull refinement. (c) Bow refinement. (d) stern refinement.

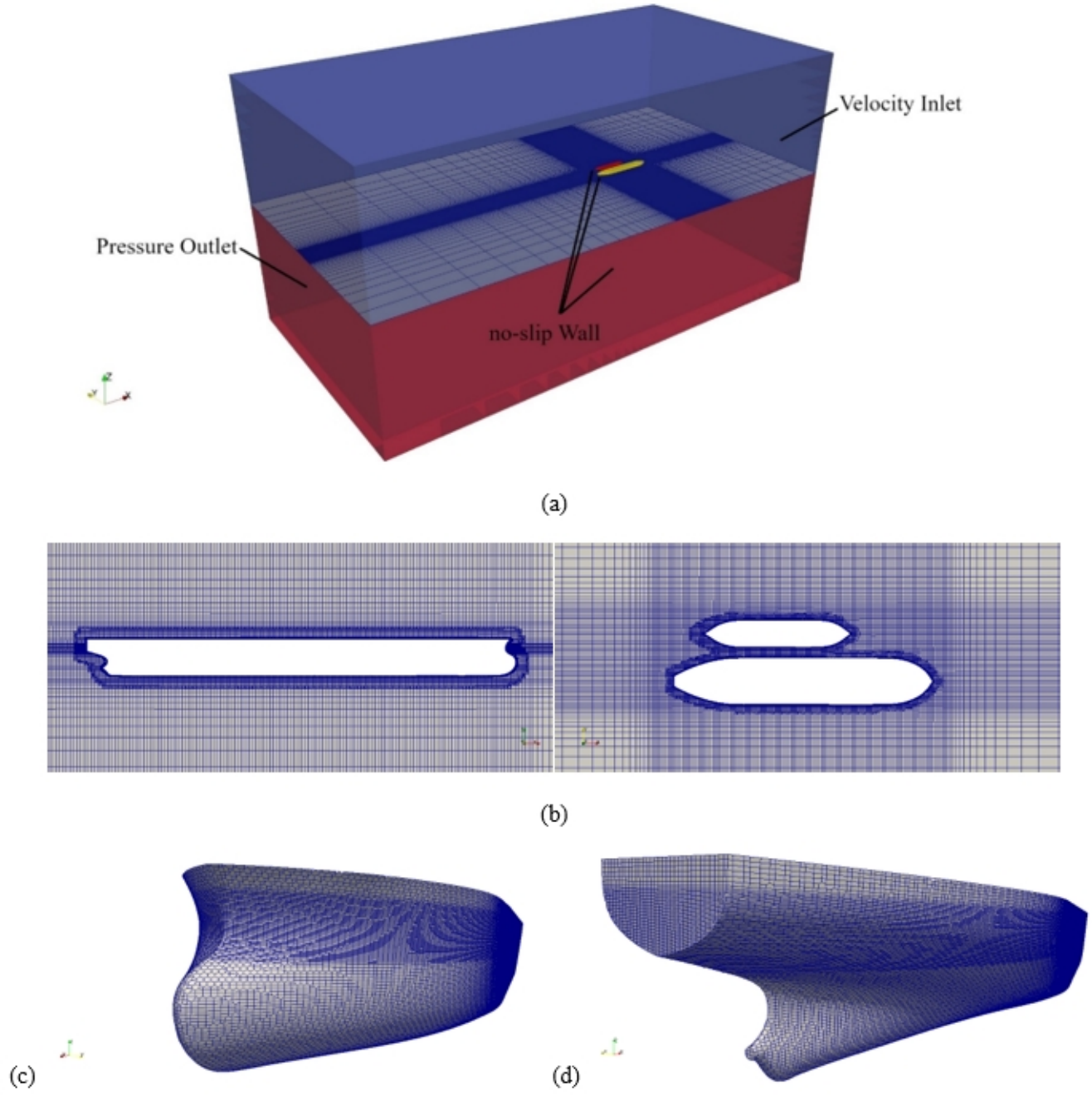

Source: Authors.

To automate the domain creation process and minimize the configuration time, a python tool, CreatMesh.py, was prepared to modify the computational grid structure according to the intended case. The generated 3-D multi-zone structured mesh is divided, depending on its discretization density, into two different zones: fine and coarse mesh. A fine zone surrounds the interacting hulls and forms the inner zone of the computational domain, and a coarser one encloses the inner zone and expands gradually away from it by 1.2 growth rate towards the domain boundaries. A general view highlighting different zones of the computational domains is shown in Fig. 3. Also, exactly as in the Decker tests, the transverse location of the STBL was in the domain's central longitudinal plane, while the SS was shifted in the lateral direction corresponding to the required non-dimensional distance η between the center-planes of the model hulls.

Viscous effects near walls are characterized by the non-dimensional wall distance $y^+ = u_t y/\upsilon$, where u_t is the friction velocity, y is the distance to the wall, and υ is the kinematic viscosity of the fluid. In this study, wall functions will be used to treat the turbulent near the walls and to approximate the viscous quantities in the boundary layer surrounding the hull surfaces. This approach of near-wall treatment allows increasing y^+ value, which decreases the grid volume and minimizes the computational time. To satisfy wall function requirements, the first grid point must be placed in the log-law region, and thus $y^+ \sim 30$ was desired to be achieved during the mesh stage. The geometrical features of the model hulls were correctly captured by snappyHexMesh with one level of refinement.

3.2. Numerical settings.

The well-known CFD packet OPENFOAM is used to simulate the turbulent viscous flow around the interacted ships and solve the Reynolds-averaged Navier-Stokes (RANS) equations. RANS equations are closed with the two-equations turbulence model K-ω SST. Finite Volume Method (FVM) is used to discrete the flow domain into a finite number of control volumes. The air-water interface is captured using the Volume of Fluid (VOF) method, (Hirt and Nichols, 1981). The discretization is performed with a linear second-order central differencing scheme for the convection and diffusion terms.

The simulation is treated as unsteady. PIMPLE, a pressure-velocity coupling algorithm based on the finite volume method is used. The total time of the simulation is adjusted to 35s. Time step is left to OPENFOAM by turning on the adjustTimeStep option. According to ITTC recommendations about the resistance computations in calm water with a low Froude number, the maximum time step is limited to 0.02s. Three iterations for each time step is used. According to the results reported by (Ali and Tryaskin, 2019), turbulence intensity T_u and eddy viscosity ratio μ_t/μ are set to 5 and 60, respectively. According to the environment of the experimental work, the water condition is modeled as fresh water at $17°C$, the corresponding value of density ρ and kinematic viscosity ν are set to $\rho = 998.8\ [kg/m^3]$ and $1.09E^{-06}\ [m^2/sec]$, respectively.

Uniform flow velocity condition is set on the inlet, a No-Slip boundary condition is set to the stationary hull surfaces immersed in the viscous fluid. Pressure values on the walls are assumed to be fixed with zero gradients. Pressure equal to atmospheric pressure is set at the outlet of the flow domain and appropriate wall functions for turbulent fields are set on hull surfaces.

Computational fluid dynamics (CFD) simulations require significant computing time along with specialized hardware. The cost of a CFD simulation consists of computational cost and 'man hours'. So, to reach the results within a reasonable timeframe, CreatMesh.py Script was used to automatically adjust the settings and prepare the mesh according to the relative position of the studied hulls, this procedure significantly reduced the preprocessing time to about 10 ∼15 minutes. Simulations were run about one month on a cluster with totally 32 GB RAM and 120 cores. Home developed scripts were used to extract and handle data during the post-processing stage.

3.3. Validations.

The experimental findings of Decker and Opheim for two hulls progressing at a close lateral distance $\eta = 1.2$ with a constant speed of 4 kt during a lightering operation in deep water, were used as benchmarks to evaluate the CFD results. A series of successive mesh smoothing was done, and the mesh that combines the accuracy of the results and the consumption of time was adopted. Fig. 4 shows a comparison between CFD, (de Decker B, 2006) and (Opheim, 2005) results.

Figure 4: CFD and Experimental results comparison for η=1.2.

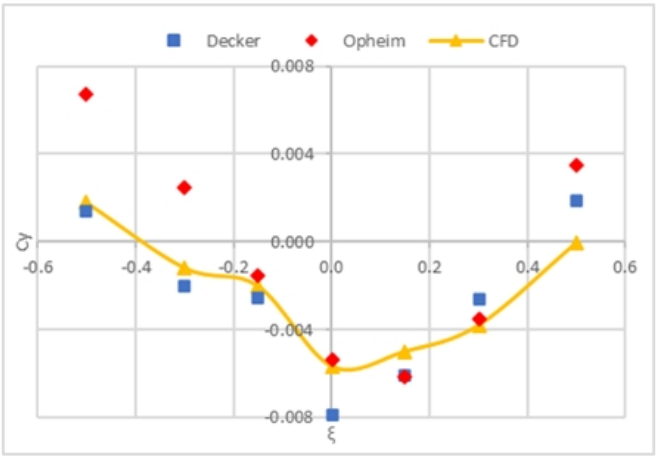

Source: Authors.

It is worth to say that both de Decker and Opheim used two models of the same type "Tanker" and different size to investigate the influence of ship speed during lightering operations, their independent experimental works were performed using the facilities at Marintek, a research institute in Trondheim, Norway.

Despite that both de Decker and Opheim conducted the same tests using the same models and test facilities but the results were clearly varied as it is shown in Fig. 4. This discrepancy in the results can be attributed to the difference in the test setup.

Opheim attached both models directly to the carriage and measured the forces immediately in both models, while Decker attached both models to each other using a rod system and measured the forces only on the ship to be lightered. Curves in Fig.4. Indicate that the results of the numerical simulations have a good agreement with Decker results in values and in the direction of influence.

4. Results

The validation presented above provides a brief view of the hydrodynamic interactions between two ships during lightering operations. Fluid flow characteristics around the ship hull in the presence of another one is governed by several parameters such as the length and area of the flow section formed between the two ships, longitudinal distance, lateral distance, length ratio, water depth etc. These parameters affect the velocity and pressure distributions near the ships simultaneously, and so the hydrodynamic interaction forces and moments. In this paper, longitudinal and lateral distances will be treated independently to ensure an exact understanding of their effects.

The details of the researched cases are presented in Table 2.

4.1. Longitudinal spacing.

4.1.1. Hydrodynamic Forces and Moment.

For a certain value of ship length ratio $L_{STBL}/L_{SS} = 1.4$, the flow surrounding two models, advancing in parallel at a constant full-scale speed of 4kt, was simulated in deep still water at various longitudinal and lateral distances.

Curves demonstrating the behavior of hydrodynamic force coefficients C_x, C_y and yaw moment coefficient C_n as a function of the longitudinal distance between STBL and SS were plotted in Fig. 5, Fig. 6 and Fig. 7.

The resistance force, F_x:

The resistance of the interacting ships varies depending on their relative longitudinal position. Within the studied range of the longitudinal distances $\xi = -0.5$ to $\xi = 0.5$, the correlation of resistance with longitudinal position may be approximated to a nonlinear relationship of the third degree with a peak at a forward position of $\xi = +0.3$. Changing the relative longitudinal position of the ships has the opposite impact on their resistance. Shifting the service ship SS from the rear to the front positions leads to a decrease in the STBL resistance, while at the same time, this action causes an increase in the SS resistance.

At any lateral distance η, the change rate of SS resistance is greater than the STBL. For transverse spacing $\eta = 1.2$, the maximum and minimum values C_x for SS are 0.0624 and 0.0229, thus the relative change in SS resistance, based on the maximum value of C_x, is about 63%, while it is only 30% for STBL. As the lateral distance ?? increases, the change rate of ship resistance decreases. The relative change of STBL resistance has a value of 30% at a transverse distance $\eta = 1.2$, while only a 26% at a transverse distance $\eta = 1.8$. Regarding SS ship, these ratios are 63% at $\eta = 1.2$ and 39% at $\eta = 1.8$.

Figure 5: Effect of longitudinal distance on resistance coefficient C_x at different values of η for both STBL and SS.

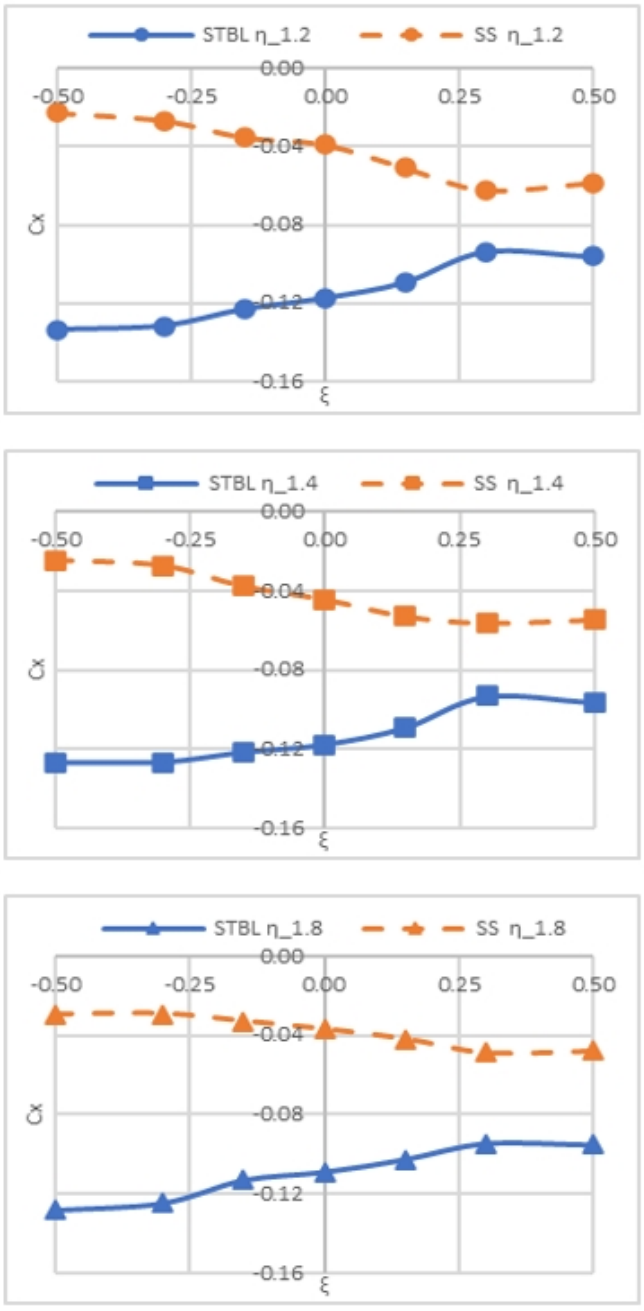

Source: Authors.

The lateral force, F_y:

The curves in Fig. 6 indicate that each of the interacting ships experiences attraction forces within a specific range of longitudinal positions, while experiences repulsion forces outside of it.

The width of the ship's attraction range decreases as the lateral distance increases. The absolute value of the hydrodynamic lateral interaction forces increases by moving away from the ends of this range.

The boundaries of the SS and STBL attraction ranges are

not corresponding. It was noticed that the width of the range of relative longitudinal positions, within which both vessels are subjected to attraction forces, decreases as the lateral distance η increases. It extends from $\xi = -0.4$ to $\xi = 0.42$ for lateral distance $\eta = 1.2$ while only from $\xi = -0.32$ to nearly $\xi = 0.28$ for $\eta = 1.4$ and disappears at $\eta = 1.8$.

Figure 6: Effect of longitudinal distance on lateral force coefficient C_y at different values of η for both STBL and SS.

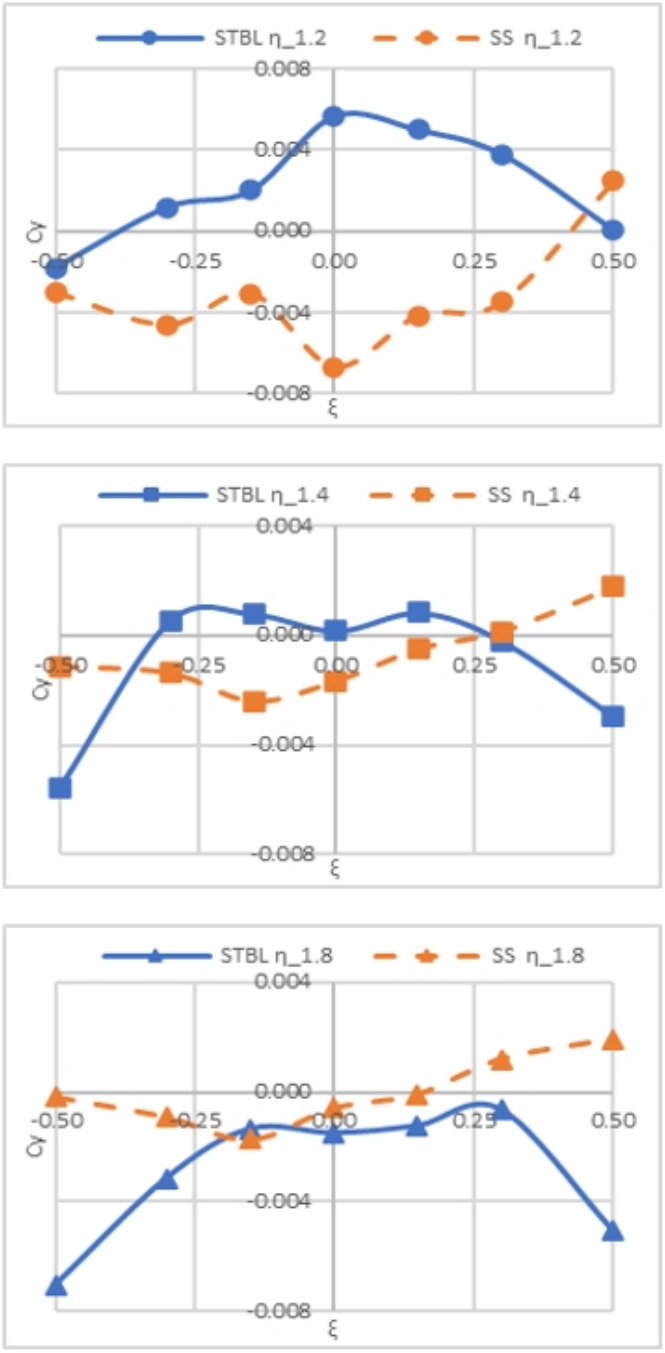

Source: Authors.

The lateral force, F_y:

The curves in Fig. 6 indicate that each of the interacting ships experiences attraction forces within a specific range of longitudinal positions, while experiences repulsion forces outside of it.

The width of the ship's attraction range decreases as the lateral distance increases. The absolute value of the hydrodynamic lateral interaction forces increases by moving away from the ends of this range.

The boundaries of the SS and STBL attraction ranges are not corresponding. It was noticed that the width of the range of relative longitudinal positions, within which both vessels are subjected to attraction forces, decreases as the lateral distance η increases. It extends from $\xi = -0.4$ to $\xi = 0.42$ for lateral distance $\eta = 1.2$ while only from $\xi = -0.32$ to nearly $\xi = 0.28$ for $\eta = 1.4$ and disappears at $\eta = 1.8$.

Dependency of the hydrodynamic interaction forces on longitudinal distance ξ could be approximated in a good agreement to a nonlinear equation of fourth degree.

The Yaw moments, N:

Within the studied range of non-dimensional longitudinal distances ξ, the yaw moment influencing the service ship SS varies linearly with the longitudinal distance. Its intensity decreases, and the direction of its influence is reversed at a negative longitudinal position $\xi < 0$, Fig. 7. The bow of the service ship SS turns towards the STBL stern at the rear longitudinal positions and rotates in the opposite direction at the forward positions. The yaw affecting the service ship SS at the rear positions is lower compared to its values at forward longitudinal positions.

Regarding the STBL, the dependency of the yaw moment impacting the STBL on the non-dimensional longitudinal distance ξ can be approximated by a nonlinear equation of the third degree characterized by the presence of the front and rear peaks, corresponding to the longitudinal positions $\xi = -0.15$ and $\xi = +0.3$. The rear peak is more intensive than the front one; the yaw decreases between them and changes its sign by approaching forward, at a positive longitudinal position $\xi > 0$. STBL bow turns away from the service ship SS at the rear positions while it rotates in the opposite direction at the forward longitudinal positions.

Generally, the bow of the rear vessel is attracted towards the stern of the front vessel, this is accompanied by a corresponding rotation of both ships in the same direction. An exception is the rear longitudinal position extended from $\xi = -0.15$ to $\xi = 0$, where the SS and STBL rotate in opposite directions.

Zero yaw moments are not compatible. So, whatever the longitudinal position is, one of the two interacting ships will be subjected to yaw moments. This result remains true over the investigated range of lateral distances.

Figure 7: Effect of longitudinal distance on yaw moment coefficient C_n at different values of η for both STBL and SS.

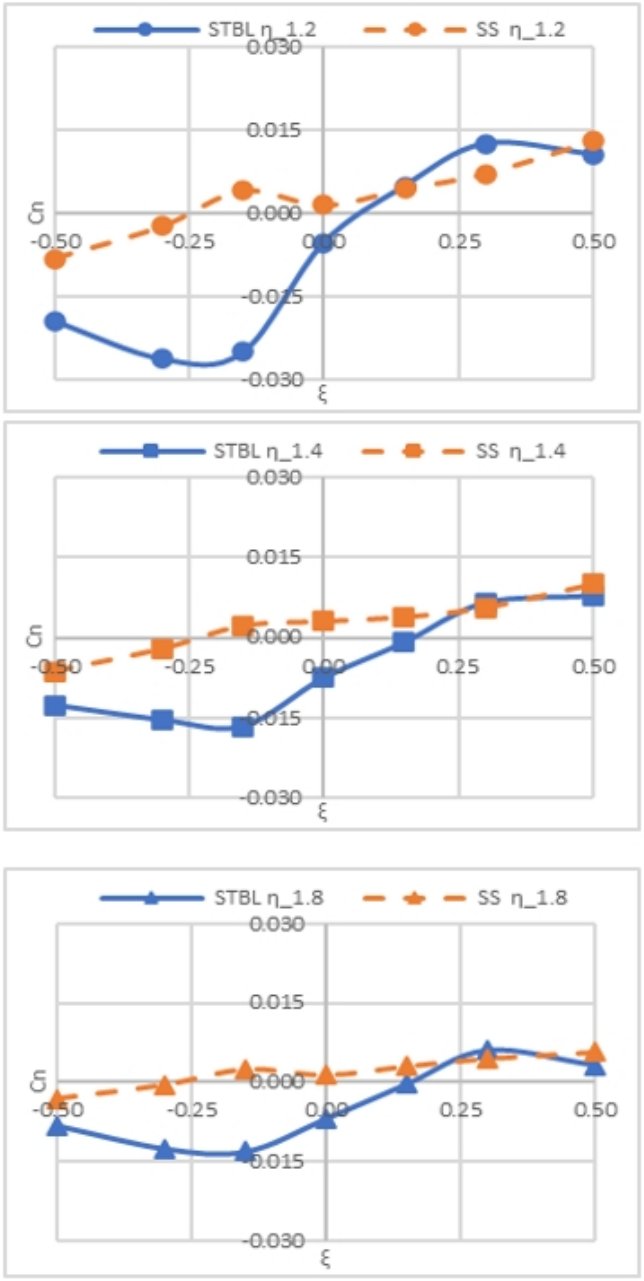

Source: Authors.

The maximum values of yaw moments decrease as the lateral distance η between the two ships increases. The range extents from $\xi = 0$ to $\xi = 0.15$ ensure relatively small yaw for both ships, and it includes, at $\eta = 1.2$, a zero-yaw moment for STBL, which make this range suitable for conducting lightering operations.

4.1.2. Wave Pattern.

Fig. 8 shows the effect of the non-dimensional longitudinal positions ξ on the wave pattern surrounding two interacting ships. Analyzing the wave contours presented in Fig.8 indicates that as the non-dimensional longitudinal position ξ changes from −0.5 to +0.5, the wave heights increase in front of the SS and decrease behind her. This simultaneous and opposite change in wave heights in front and behind the SS leads to an increase in her wave resistance. However, this change in ξ has a smaller effect on the STBL wave contour.

Furthermore, the bow of the rear vessel and the stern of the front vessel are subjected to the influence of a low-pressure area, indicated by the trough formed between the interacting ships, which explains the increase in the resistance of the interacting ship at the forward positions compared to her resistance at the rear positions.

4.1.3. Surface pressure.

To properly understand the mechanism of the formation of the hydrodynamic force, its intensity, point of impact, and direction of influence, it is necessary to study the pressure distribution for each hull separately. Also, it is necessary to study and compare the pressure distribution on both sides of the hull involved in the case of interaction with another one. Studying the pressure distribution only on the facing surfaces of the interacting ships is not enough to properly understand the phenomenon. For this aim, the pressure distribution over the submersed surfaces of the two interacting ships SS and STBL, advancing in parallel at a lateral distance $\eta = 1.2$, are presented on Fig. 9 for different values of ξ.

The intensity of the pressure affecting a certain surface of the hull, the areas of the surface subjected to a certain pressure value, the location of this surface in relation to the ship's center of gravity, all these factors collectively affect the resulted hydrodynamic force and its moment.

For $\xi = -0.5$, for example, the difference in pressure on both sides of the STBL stern, in addition to the presence of high pressure on the port side of her mid-hull, leads to the formation of a negative hydrodynamic force. The resulted hydrodynamic force acts in front of the STBL center of gravity and generates a negative yaw moment that causes the STBL stern to rotate toward the SS bow.

For position $\xi = -0.3$, a positive pressure is concentrated on the port side of the STBL mid-hull, but the surface area exposed to negative pressure on the STBL stern port is larger, and the pressure value on stern port is lower than on the stern starboard. Thus, the hydrodynamic force is a positive lateral force that acts on the rear part of the STBL hull, behind her center of gravity. So, this lateral force generates a negative yaw moment and causes the STBL stern to rotate toward the SS bow. The behavior of STBL and SS for different values of ξ is discussed in the same way.

4.2. Lateral spacing.

The yaw moments affecting the interacting ships have minimum values within the range of longitudinal positions extends from ξ= 0 to ξ= 0.15 while reach critical values outside of this range. Therefore, two different longitudinal positions outside of this range ξ=∓0.3 were selected to present the effect of lateral spacing η on the hydrodynamic interaction forces and moments as well as on the wave pattern and surface pressure distribution.

Figure 8: Effect of longitudinal distance of SS on wave pattern at η=1.2, ($\xi = -0.5 \sim 0.5$).

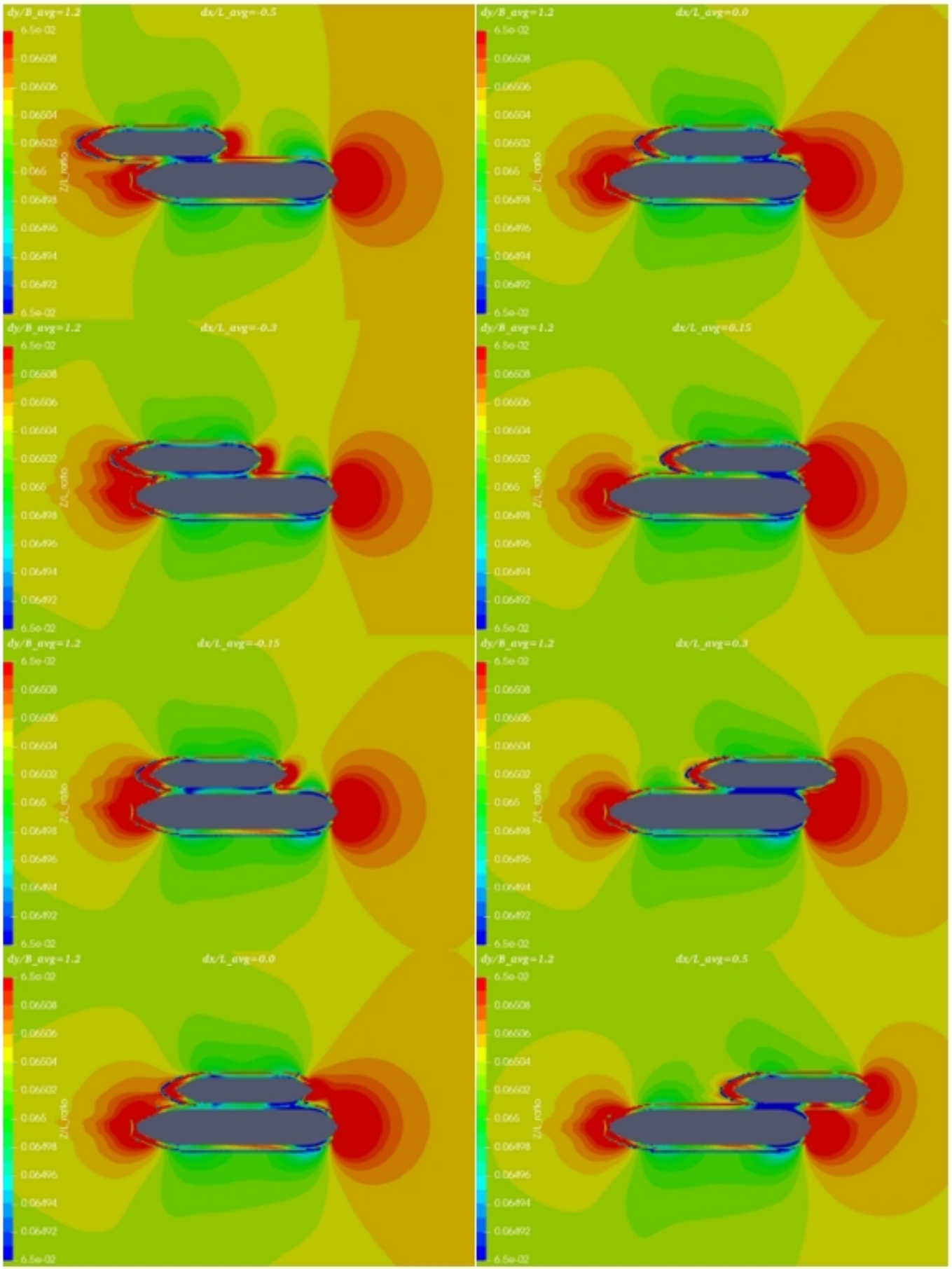

Source: Authors.

Figure 9: Effect of longitudinal distance on surface pressure distribution for η=1.2, ($\xi = -0.5 \sim 0.5$).

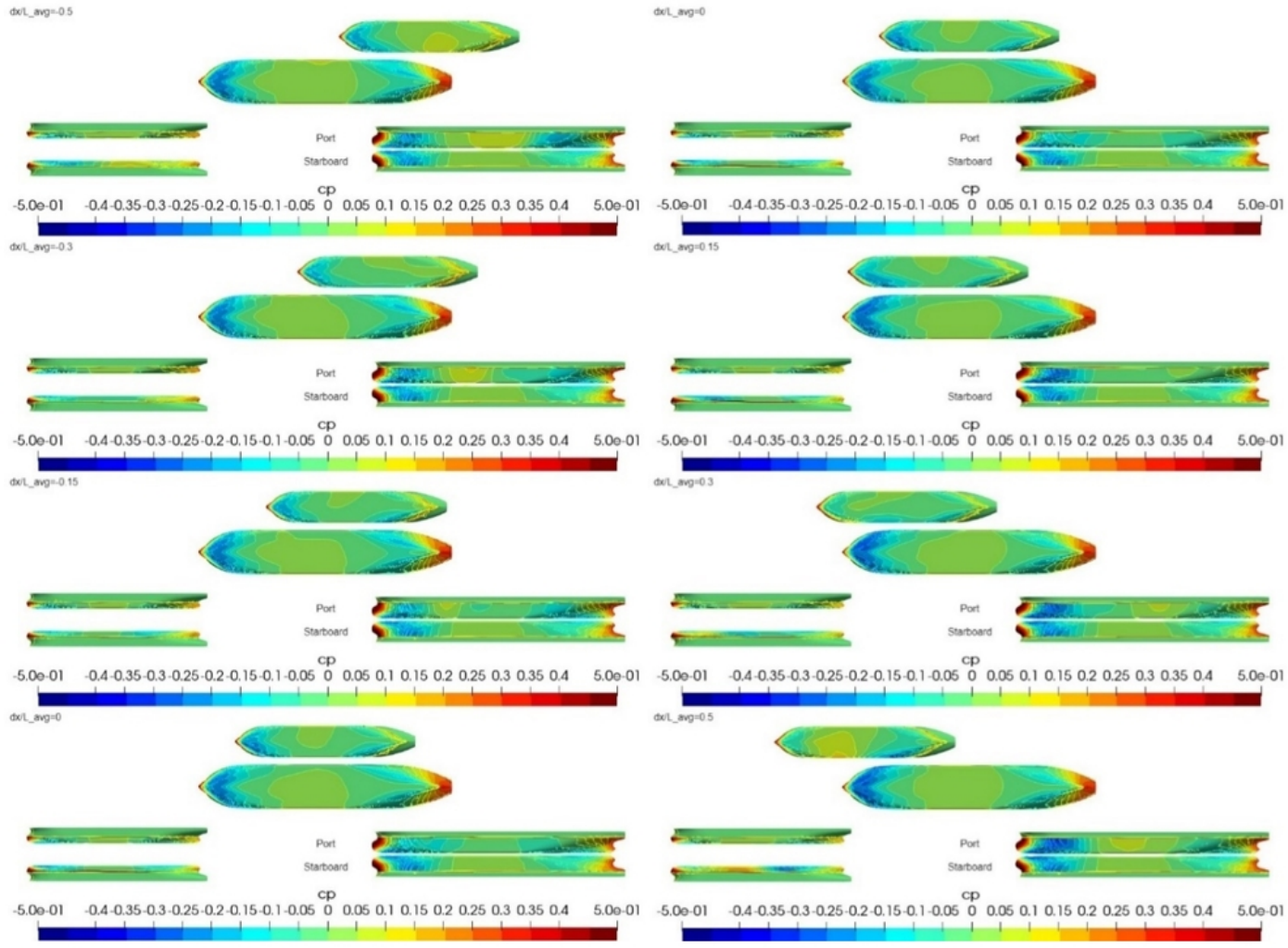

Source: Authors.

4.2.1. Hydrodynamic Forces and Moment.

The resistance force, F_x:

The curves in Fig. 10 indicate that, within the studied range of transverse distance, increasing the lateral distance η oppositely affects the two ships. For rear longitudinal position $\xi = -0.3$, increasing the transverse distance η leads to a decrease in the STBL resistance while it leads to an increase in the SS resistance. Increasing the lateral distance from $\eta = 1.06$ to $\eta = 1.8$ causes a decrease in the resistance forces by 14% on STBL and an increase by 13% on SS.

For front longitudinal positioning $\xi = +0.3$, the opposite effect on the resistance of the two ships remains dominant. However, increasing the lateral distance causes an increase in the STBL resistance while causes a decrease in the SS resistance. Increasing the lateral distance from $\eta = 1.06$ to $\eta = 1.8$ causes an increase in the resistance forces by 8% on STBL and a decrease by 28% on SS.

The lateral force, F_y:

The C_y curves of STBL show that as the lateral distance η decreases, the repulsion forces gradually decrease and turn into attraction forces. Curves show a noticeable change in the intensity of the attraction forces in the range $\eta = 1.2$ to $\eta = 1.06$. In this range attraction forces increases at rear positioning $\xi = -0.3$ while decease at forward positioning $\xi = +0.3$.

However, more points are required to accurately define the behavior of attraction forces in this range. Forces affect SS exhibit a same behavior.

The Yaw moments, N:

The curves in Fig. 12 show that both ships, STBL and SS, rotate in the same direction regardless of whether the longitudinal position is $\xi = -0.3$ or $\xi = 0.3$. Generally, the yaw moments affecting both ships decrease as the transverse distance η between their centerlines increases. This is clearly shown at the rear position $\xi = -0.3$, but for the forward position $\xi = 0.3$, a noticeable change in STBL yaw behavior is observed within the range $\eta = 1.06$ to $\eta = 1.2$. Adjusting the yaw behavior within this range requires more points.

Figure 10: Effect of lateral distance on resistance coefficient C_x at different values of ξ for both STBL and SS.

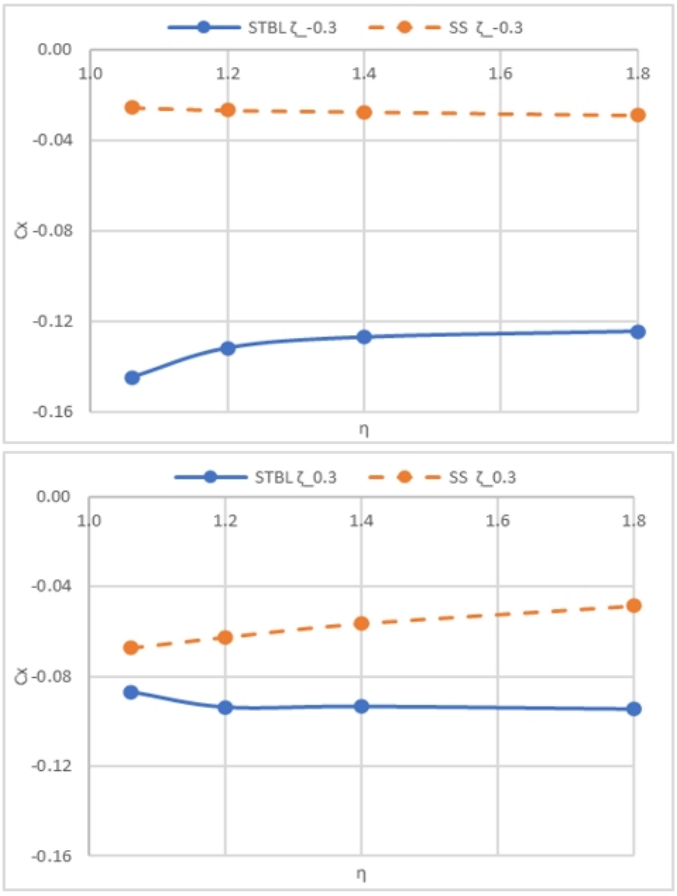

Source: Authors.

Figure 11: Effect of lateral distance on lateral force coefficient C_y at different values of ξ for both STBL and SS.

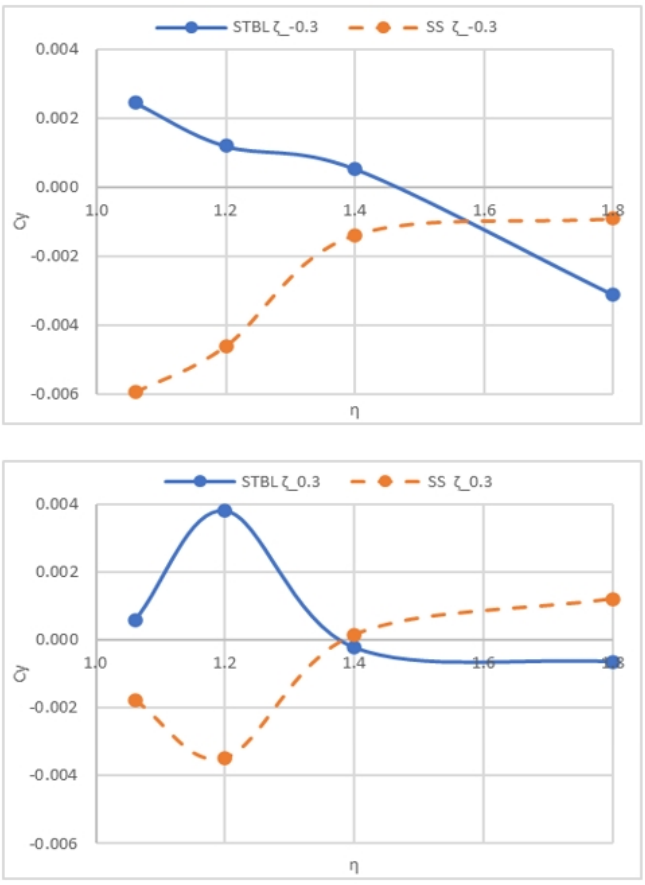

Source: Authors.

4.2.2. Wave Pattern.

The presence of ships close to each other leads to a decrease in the height of the waves between them, which forms a trough that connects the opposite surfaces of the two interacting ships. As the transverse distance between the two ships increases, the height of this trough decreases, indicating an increase in pressure, which in turn leads to an increase in the resistance of the rear ship and a decrease in the resistance of the front ship, Fig. 13.

4.2.3. Surface pressure.

Fig. 14 shows the change in pressure with increasing transverse distance η at two values of the longitudinal position $\xi = -0.3$ and $\xi = 0.3$.

For $\xi = -0.3$, reviewing the pressure distribution on STBL surface at $\eta = 1.06$ show that the surface area exposed to the negative pressure is greater on the STBL port side than on starboard side, and its intensity is also higher, which makes the STBL subjected to a positive hydrodynamic force. As the transverse distance η increase, the pressure intensity on the STBL port side (both positive and negative) decreases and therefore the pressure difference between port and starboard surfaces decreases, which explains the resulted decrease in the lateral hydrodynamic force. The effect of lateral distance on pressure distribution on SS and STBL surfaces at $\xi = 0.3$ is discussed in the same way.

Conclusions.

The bow and stern of the ship are surrounded by two high-pressure areas, while each side of the parallel body of the ship advancing in calm weather conditions is surrounded by a low-pressure area. These areas are considered distinctive signs of flow around the hull of the ship. As the non-dimensional longitudinal position of the interacted vessels changes, these pressure areas overlap with each other and therefore their distribution around the body differs causing a difference in the flow velocity between the port and starboard sides of the hull for each ship, which leads to changes in the values and directions of the hydrodynamic forces and moments.

OPENFOAM, an open-source CFD packet was used to simulate the hydrodynamic interaction forces and moments affecting during lightering operation between two KVLCC2 hulls advancing at low Froud number in deep water and calm weather with the same speed. RANS method was used for turbulence modeling, k-ω SST turbulent model was used to close RANS equations.

Figure 12: Effect of lateral distance on yaw moment coefficient C_n at different values of ξ for both STBL and SS.

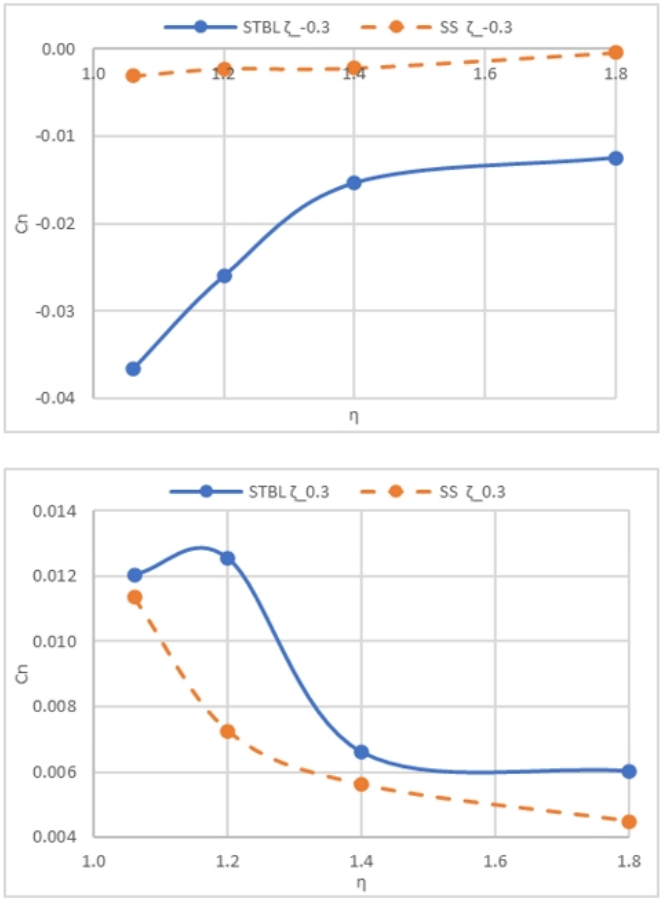

Source: Authors.

A series of systematic computations were performed to investigate the influence of the relative longitudinal and transverse distances on the hydrodynamic interaction forces and moments. Numerical results were validated by experimental results. The changes in the hydrodynamic forces and moments as a function of the longitudinal and transverse spacing were simulated and analyzed.

A noticeable change in the hydrodynamic forces and moments was observed within the range of the lateral distances $\eta = 1.06$ to $\eta = 1.2$. Adjusting the hydrodynamic behavior within this range requires more points and thus additional subsequent investigation is required.

The following results were obtained for ship length ratio 1.4, and longitudinal distances $\xi = -0.5$ to $\xi = 0.5$.

Longitudinal spacing:

F_x: There is no ideal longitudinal location for the ship's resistance since altering the longitudinal position oppositely affects the resistance of the interacting ships. The service ship SS is more influenced by altering the longitudinal position than the ship to be lightered STBL. The interacting ship has a lower resistance when she is located at rear positions than at front positions, whatever she is "SS" or "STBL".

F_y: The intensity and direction of the lateral hydrodynamic force exerted on each ship change as the longitudinal position varies. The interacting ships experience maximum attraction force at longitudinal position $\xi = 0$. Each ship has a range of longitudinal positions; within it, the ship is subjected to an attraction force, while outside of this range, she is subjected to a repulsion force. As the non-dimensional lateral distance η increases, the width of the attraction range decreases until it vanishes.

The boundaries of the attraction ranges of the interacting ships are not corresponding. The range of longitudinal positions where both ships are subjected to attraction forces disappears at lateral distance $\eta = 1.8$.

N: Zero yaw moments of the interacting ships are not corresponding. Therefore, whatever the longitudinal position, at least one of the interacting ships will be subjected to yaw moment. The bow of the rear vessel is attracted towards the front vessel stern; this is accompanied by a corresponding rotation of both ships in the same direction. An exception is the rear longitudinal position extended from $\xi = -0.15$ to $\xi = 0$, where the SS and STBL rotate in opposite directions. Yaw moments of both ships decrease as lateral distance increases.

Lateral spacing:

F_x: Changing the lateral distance differently affects the resistance of the interacting ships, both at front and rear longitudinal positions. For rear positions of SS, increasing the lateral distance will increase her resistance while decrease the STBL resistance. An opposite interaction will occur when SS is located at front longitudinal positions.

F_y: Decreasing the lateral distance between the interacting ships will turn the repulsion forces into attraction forces. The attraction force increases as the lateral distance decreases.

N: Lateral distance has a similar effect on the yaw moments of the interacting ships, both at front and rear longitudinal positions. Increasing lateral distance will decrease yaw moments of both STBL and SS.

Nonetheless, these results must be interpreted with caution and a possible primary limitation should be borne in mind. The ship length ratio has a major effect on the velocity and pressure field distribution around the interacting ships, and so, on the wave pattern and boundary layer characteristics. Therefore, the effects of this factor on the interacting ships during lightering operation could be addressed in future research.

References.

Ali, R., Tryaskin, N.V., 2019. Numerical study on effect of the turbulence initial conditions on transition flow over 2D airfoil. Proceedings of the Institute for System Programming of the RAS 31, 203–214. https://doi.org/10.15514/ISPRAS-2019-31(6)-13

Benedict, K., Köpnick, W., Baldauf, M., Gronarz, A., Friedhoff, B., de Mello Petey, F., 2011. Improved simulation model and methods for determination of the required passing distance between ships in restricted fairways, in: RINA, Royal Institution of Naval Architects - 2nd International Conference on Ship

Figure 13: Effect of lateral distance on wave pattern. (a) ξ= −0.3. (b) ξ= +0.3.

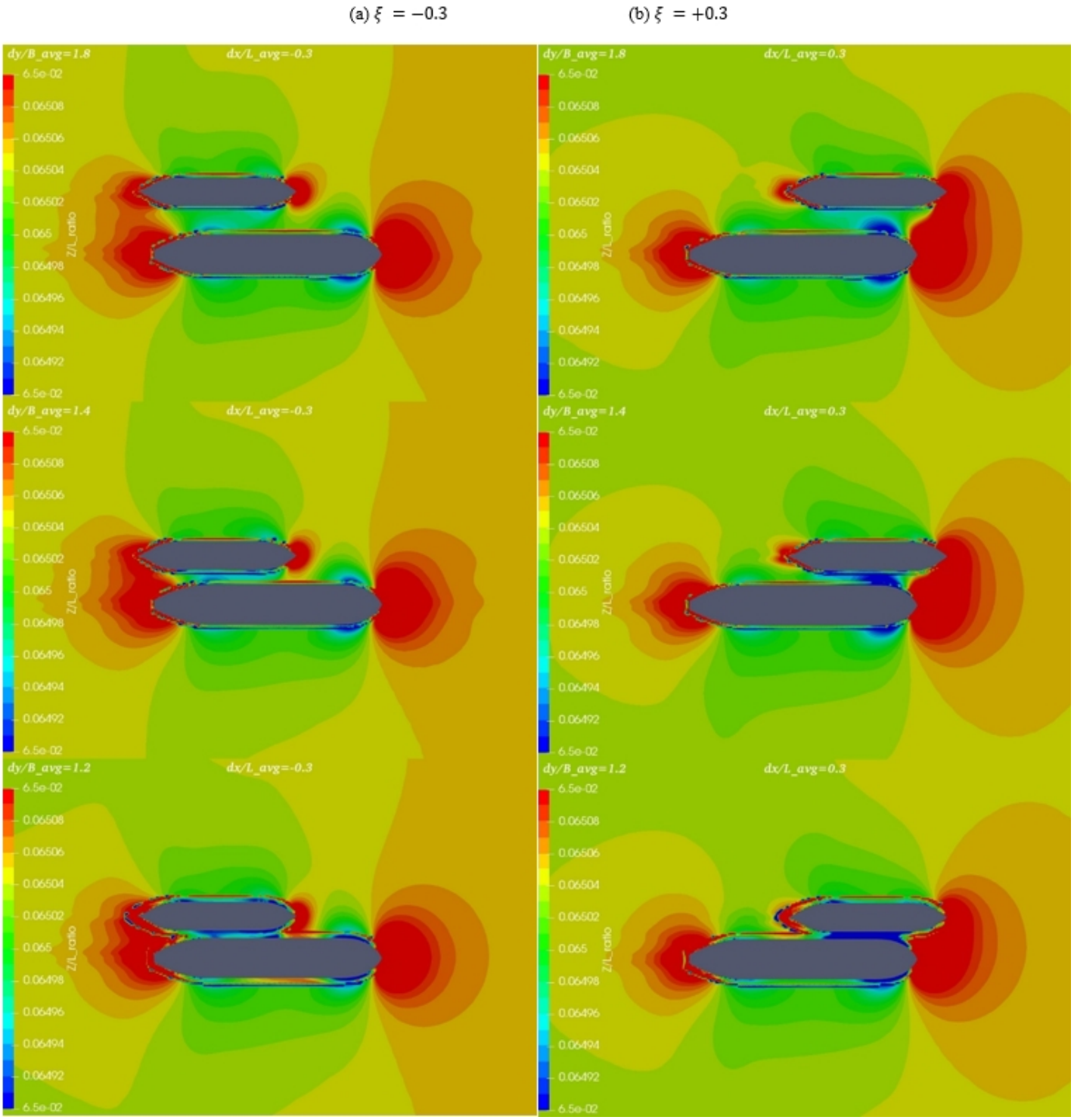

Source: Authors.

Figure 14: Effect of lateral distance on surface pressure distribution. (a) ξ= −0.3. (b) ξ= +0.3.

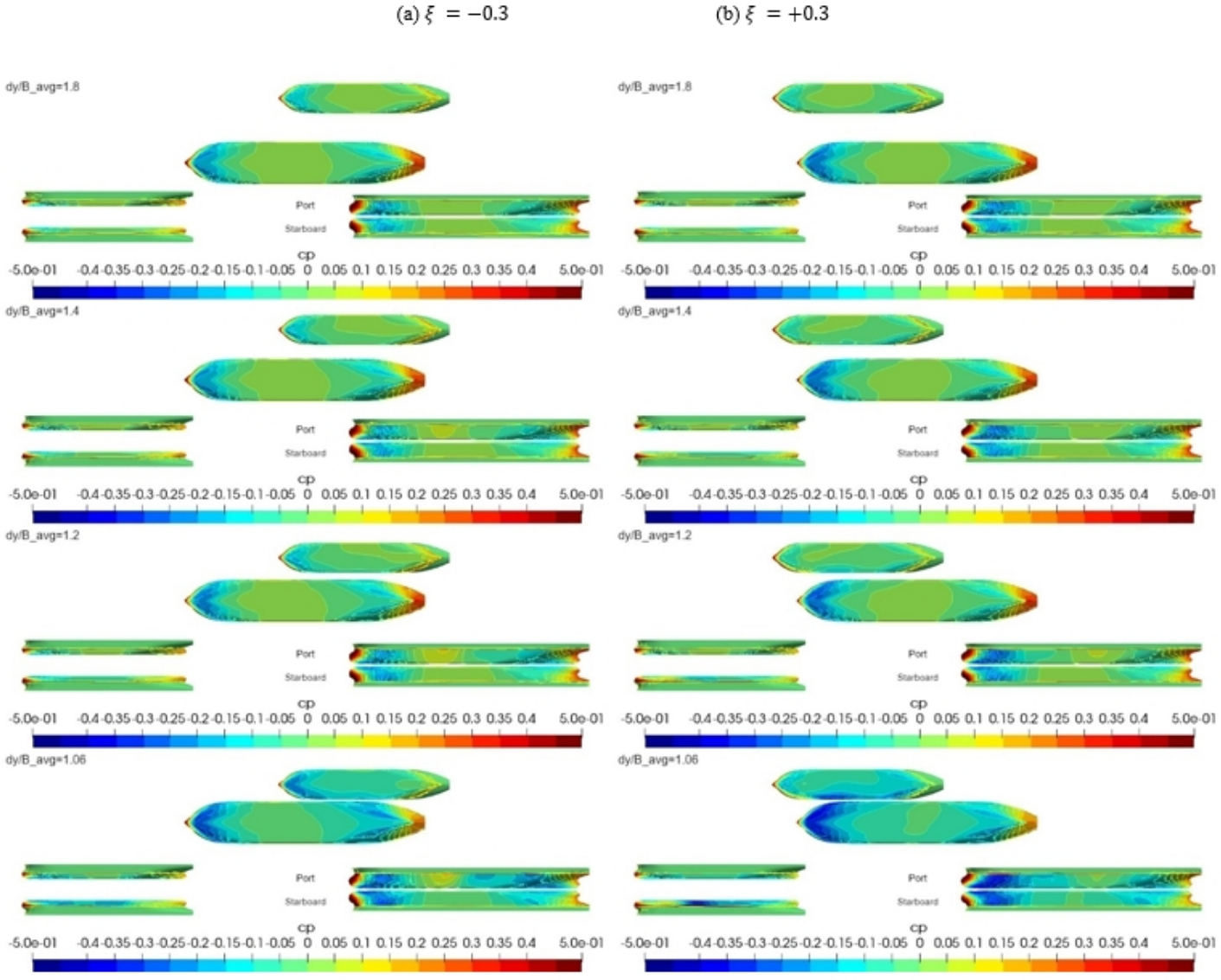

Source: Authors.

Manoeuvering in Shallow and Confined Water: Ship to Ship Interactions 2011.

de Decker B, 2006. Ship-Ship Interaction during Lightering Operations. Ghent.

Hirt, C.W., Nichols, B.D., 1981. Volume of fluid (VOF) method for the dynamics of free boundaries. Journal of Computational Physics 39. https://doi.org/10.1016/0021-9991 (81) 90145-5

Nandhini, V., Nallayarasu, S., 2020. CFD simulation of the passing vessel effects on moored vessel. Ships and Offshore Structures 15. https://doi.org/10.1080/17445302.2019.1606764

Opheim, 2005. Experimental investigation of ship to ship interaction in lightering operations. Journal of Ship Research.

Serban, S., 2015. Case Study of Ship Squat in Sulina Channel Using NTPRO 5000 Navigational Simulator. Applied Mechanics and Materials 809–810, 1193–1198. https://doi.org/10.-4028/www.scientific.net/AMM.809-810.1193

Sian, A.Y., Maimun, A., Ahmed, Y., Rahimuddin, 2016. SIMULTANEOUS SHIP-TO-SHIP INTERACTION AND BANK EFFECT ON A VESSEL IN RESTRICTED WATER, in: Proceedings of the 4th International Conference on Ship Manoeuvring in Shallow and Confined Water (MASHCON), 23 - 25 May 2016, Hamburg, Germany.

Skejic, R., Xiang, X., Faltinsen, O., Berg, T.E., 2011. HYDRODYNAMIC INTERACTION LOADS BETWEEN TWO SHIPS DURING LIGHTERING OPERATION IN CALM WATER.

WANG, Q.X., 2007. An analytical solution for two slender bodies of revolution translating in very close proximity. Journal of Fluid Mechanics 582, 223–251. https://doi.org/10.1017/S002-2112007005824

Wnęk, A.D., Sutulo, S., Guedes Soares, C., 2018. CFD

Analysis of Ship-to-Ship Hydrodynamic Interaction. Journal of Marine Science and Application 17. https://doi.org/10.1007/s11804-018-0010-z

Xiang, X., Faltinsen, O.M., 2010. Maneuvering of two interacting ships in calm water, in: 11th International Symposium on Practical Design of Ships and Other Floating Structures, PRADS 2010. https://doi.org/10.1007/bf03449294

Yao, J.X., Zou, Z.J., 2010. Calculation of ship squat in restricted waterways by using a 3D panel method, in: Journal of Hydrodynamics. https://doi.org/10.1016/S1001-6058(09) 6024-1-9

Yu, D., Wang, L., Yeung, R.W., 2019. Experimental and numerical study of ship-to-ship interactions in overtaking manoeuvres. Proceedings of the Royal Society A: Mathematical, Physical and Engineering Sciences 475, 20180748. https://doi.org/10.1098/rspa.2018.0748

Yuan, Z.M., He, S., Kellett, P., Incecik, A., Turan, O., Boulougouris, E., 2015. Ship-to-ship interaction during overtaking operation in shallow water. Journal of Ship Research 59. https://doi.org/10.5957/JOSR.59.3.150004

Yuan, Z.-M., Incecik, A., 2016. Investigation of Ship-Bank, Ship-Bottom and Ship-Ship Interactions by Using Potential Flow Method, in: Proceedings of the 4th International Conference on Ship Manoeuvring in Shallow and Confined Water (MASHCON), 23 - 25 May 2016, Hamburg, Germany.

Zhang, C.X., Zou, Z.J., 2011. Numerical investigation on ship-ship hydrodynamic interaction in restricted waters, in: RINA, Royal Institution of Naval Architects - 2nd International Conference on Ship Manoeuvering in Shallow and Confined Water: Ship to Ship Interactions 2011.